Forest Ecology and Management 433 (2019) 364–375

Contents lists available at ScienceDirect

Forest Ecology and Management

journal homepage: www.elsevier.com/locate/foreco

Leaf area density from airborne LiDAR: Comparing sensors and resolutions in a temperate broadleaf forest ecosystem

Aaron G. Kamoske[a,*], Kyla M. Dahlin[a,b], Scott C. Stark[c], Shawn P. Serbin[d]

[a] Michigan State University, Department of Geography, Environment, & Spatial Sciences, 673 Auditorium Rd. #116, East Lansing, MI 48824, United States
[b] Michigan State University, Program in Ecology, Evolutionary Biology, & Behavior, 103 Giltner Hall, 293 Farm Lane #103, East Lansing, MI 48824, United States
[c] Michigan State University, Department of Forestry, 480 Wilson Rd #126., East Lansing, MI 48824, United States
[d] Brookhaven National Laboratory, Environmental and Climate Sciences Department, 98 Rochester St, Upton, NY 11973, United States

ARTICLE INFO

Keywords:
Airborne LiDAR
Leaf area density
Leaf area index
Forest structure

ABSTRACT

Forest processes that play an essential role in carbon sequestration, such as light use efficiency, photosynthetic capacity, and trace gas exchange, are closely tied to the three-dimensional structure of forest canopies. However, the vertical distribution of leaf traits is not uniform; leaves at varying vertical positions within the canopy are physiologically unique due to differing light and environmental conditions, which leads to higher carbon storage than if light conditions were constant throughout the canopy. Due to this within-canopy variation, three-dimensional structural traits are critical to improving our estimates of global carbon cycling and storage by Earth system models and to better understanding the effects of disturbances on carbon sequestration in forested ecosystems. In this study, we describe a reproducible and open-source methodology using the R programming language for estimating leaf area density (LAD; the total leaf area per unit of volume) from airborne LiDAR. Using this approach, we compare LAD estimates at the Smithsonian Environmental Research Center in Maryland, USA, from two airborne LiDAR systems, NEON AOP and NASA G-LiHT, which differ in survey and instrument specifications, collections goals, and laser pulse densities. Furthermore, we address the impacts of the spatial scale of analysis as well as differences in canopy penetration and pulse density on LAD and leaf area index (LAI) estimates, while offering potential solutions to enhance the accuracy of these estimates. LAD estimates from airborne LiDAR can be used to describe the three-dimensional structure of forests across entire landscapes. This information can help inform forest management and conservation decisions related to the estimation of aboveground biomass and productivity, the response of forests to large-scale disturbances, the impacts of drought on forest health, the conservation of bird habitat, as well as a host of other important forest processes and responses.

1. Introduction

With terrestrial ecosystems storing around 11 gigatonnes of atmospheric carbon dioxide (CO_2) per year, approximately one third of anthropogenic emissions, forests are a critical component of the Earth's carbon cycle (Le Quere et al., 2015; Pan et al., 2011b). Forest processes that play an essential role in carbon sequestration are closely related to the three-dimensional structure of forest canopies (Parker et al., 2004; Hardiman et al., 2011). The horizontal and vertical distribution of foliage within a canopy directly and indirectly regulates the canopy-scale light use efficiency (LUE, Ellsworth and Reich, 1993; Kitajima, 2004), photosynthetic capacity, and exchanges of water vapor, CO_2, and other trace gases (Baldocchi et al., 1988) in a number of important ways, including by defining the within-canopy radiation regime (Meir et al., 2002; Niinemets, 2007) and turbulence environment. This variability, in turn, has significant impacts on forest productivity and thus carbon storage (Hardiman et al., 2013). However, these relationships are not static in 2- or 3-dimensional space; leaf physiological traits vary across landscapes (Serbin et al., 2014) and leaves at varying vertical positions within the canopy are physiologically unique due to differing light environments (Poorter et al., 2009). Given differences in leaf physiology and morphology, a better knowledge of how these properties vary vertically and horizontally within the canopy will provide a better estimate of carbon storage (Niinemets et al., 2015). Due to this within-canopy variation of light and foliar traits, inclusion of the three-dimensional structural diversity of a forest canopy is critical to making improvements to carbon storage estimates by Earth system models (ESMs) (Bonan et al., 2012).

* Corresponding author.
E-mail addresses: kamoskea@msu.edu (A.G. Kamoske), kdahlin@msu.edu (K.M. Dahlin), scstark@msu.edu (S.C. Stark), sserbin@bnl.gov (S.P. Serbin).

https://doi.org/10.1016/j.foreco.2018.11.017
Received 21 August 2018; Received in revised form 9 November 2018; Accepted 10 November 2018

The structural diversity within a canopy and across a landscape is a critical component of ecological models that scale processes from leaf to landscape (Jarvis and McNaughton, 1986). Currently, many of these models, such as the Community Land Model, treat the canopy as only having two types of leaves – sunlit and shaded (Bonan et al., 2014). This lack of information about the three-dimensional canopy is one of a host of factors contributing to the uncertainty and disparity in predicting carbon uptake by terrestrial ecosystems (Fisher et al., 2018). By incorporating this vertical and horizontal structure, models can provide a better representation of forested landscapes, thus reducing model uncertainty and improving estimates of ecosystem productivity and landscape-scale functions (Bonan et al., 2014). However, the benefits of accurately measuring the three-dimensional structure of a forest canopy are not limited to ESMs.

Understanding the effects of disturbances on forested ecosystems is vital to long-term quantification of carbon storage (Goodale et al., 2002; Pan et al., 2011a). Defoliation from invasive insects and pathogens (Hummel and Agee, 2003), stand replacement and thinning from fire (Collins et al., 2011), stress and mortality from drought (Anderegg et al., 2013), gap creation from wind (Hanson and Lorimer, 2007), and a host of other disturbance impacts can affect the structure of a forest. Moreover, these changes in forest structure can significantly affect ecosystem processes related to carbon uptake (Gough et al., 2013). With forest managers facing increasingly complex disturbances, the ability to map and measure forest structure across landscapes is critical to developing forest management plans that consider the impacts of these disturbances on forest health, resilience, and function (Becknell et al., 2015).

While well-established field-based methods to measure the vertical and horizontal distribution of leaves within an individual tree's canopy exist, applying these methods at a landscape scale is challenging due to time, labor, and access constraints (Zheng and Moskal, 2009). These measurements are made primarily by two methodologies (Hosoi and Omasa, 2007); by lowering a probe through the canopy and recording the height and frequency of foliage contact with the probe (e.g. inclined point quadrat method; Wilson, 1960) or by using a telephoto lens to measure the proportion of leaves in a given area at set height intervals looking up into the canopy (e.g. canopy closure method; MacArthur and Horn, 1969). These methodologies are ultimately used to estimate leaf area index (LAI; the one-sided leaf area per unit of ground area; Chen and Black, 1992) and leaf area density (LAD; the total leaf area per unit of volume; Weiss et al., 2004) which provide critical information about ecosystem processes and functions related to forest structure (Detto et al., 2015). The estimation of these variables is influenced by a variety of factors, including the assumption that leaves are distributed randomly throughout the canopy and the scale at which the measurements were taken. For example, the distribution of clusters of leaves, stems, and branches, the spatial structure of gaps in the forest, and the disturbance histories of a landscape (Silva et al., 2017) may influence the error and bias of forest structural estimates depending on the sampling scale used (e.g. an individual tree, a plot, or a forest stand; Roussel et al., 2017). However, emerging technologies present opportunities to evaluate factors influencing LAI and LAD estimates and to overcome prior limitations to extracting this critical information across landscapes, at varying temporal resolutions and with high accuracy.

Airborne light detection and ranging (LiDAR) directly measures the distance between a sensor and an object using laser pulses. LiDAR sensors provide a high repetition rate of these measurements (as high as 33,000 pulses per second) and when applied to forests these LiDAR pulses act as a canopy probe, allowing for the estimation of the three-dimensional internal structure of a forest canopy (Lefsky et al., 2002). In contrast, traditional passive optical remote sensing systems (e.g. Landsat) produce two-dimensional images of sunlight reflected off the top of the canopy, which does not capture the complex vertical and horizontal structure of a forest canopy (Morsdorf et al., 2006). LiDAR derived structural measurements have the potential to improve the accuracy and resolution of studies that have traditionally relied on two-dimensional remote sensing or field surveys, including estimates of defoliation from invasive pests and pathogens (Meng et al., 2018), predicting above ground carbon dynamics (Taylor et al., 2015; Stark et al., 2012, 2015), measuring forest stand successional stages (Falkowski et al., 2009), within-canopy habitat modeling (Smart et al., 2012), and ecosystem trait upscaling (Antonarakis et al., 2014). Additionally, with a host of applications LiDAR data are becoming more widely available at larger spatial and temporal scales.

In the United States, two airborne systems are acquiring publicly available LiDAR data at a wide-range of locations covering many ecoregions with increasing frequency. The National Ecological Observatory Network's Airborne Observation Platform (Kampe et al., 2010; NEON AOP) collected airborne data at more than 60 sites throughout the United States in 2018 (its first year of full operations), with survey areas ranging from 100 to 300 km^2 around each site. Data will be collected at NEON sites on a semi-annual basis for the next 30 years, offering an unprecedented opportunity to address long-term ecological questions (Hinckley et al., 2016). NASA Goddard's LiDAR, Hyperspectral & Thermal Imager (NASA G-LiHT) is another airborne system, which currently flies site-specific missions for NASA-funded studies (Cook et al., 2013), with data publicly available in over 30 US states and territories and several countries dating back to 2011. With the launch of the NEON AOP and the continuing collection by NASA G-LiHT, LiDAR is becoming more readily available than ever before. This abundance of data will further grow with the launch of NASA's Global Ecosystem Dynamics Investigation (GEDI) system on the International Space Station, which will provide waveform LiDAR coverage of temperate and tropical forests between 51 degrees North and South, beginning in late 2018 (Stavros et al., 2017). While LiDAR data are becoming more available at wider spatial extents and temporal scales, a critical gap remains between landscape and macrosystem ecologists who want to ask questions at broad spatial scales and remote sensing scientists who are more familiar with the opportunities and challenges of using these data (Turner et al., 2015; Pettorelli et al., 2014; Mairota et al., 2015).

In this study, we help address this gap by describing a reproducible and open-source methodology for estimating LAD and LAI from airborne LiDAR. We compare LAD estimates derived from publicly available point cloud data produced by the NEON AOP and NASA G-LiHT LiDAR systems, which differ in survey and instrument specifications, collection goals, and laser pulse densities. Furthermore, we use hemispherical photographs as a means to calibrate our LiDAR derived LAD and LAI estimates. We also address the impacts of the spatial scale of analysis and differences in canopy penetration and pulse density on LAD and LAI estimates while offering potential solutions to enhance the accuracy of these estimates.

2. Materials and methods

2.1. Study site

Field measurements and LiDAR data were acquired at the Smithsonian Environmental Research Center (SERC), approximately 16 km south of Annapolis, Maryland, USA (Fig. 1). SERC is a relocatable terrestrial NEON (neonscience.org) site and contains a mixed-species deciduous forest with American sweetgum (*Liquidambar styraciflua*) and tulip tree (*Liriodendron tulipifera*) dominating the overstory. Mockernut hickory (*Carya tomentosa*), white oak (*Quercus alba*), and American beech (*Fagus grandifolia*) are also common, with ironwood (*Carpinus caroliniana*) and other small tree species forming a dense understory (Parker, 1995). SERC contains approximately 11 km^2 ranging in elevation from zero to 40 m above sea level, and with slopes ranging from zero to 34 degrees.

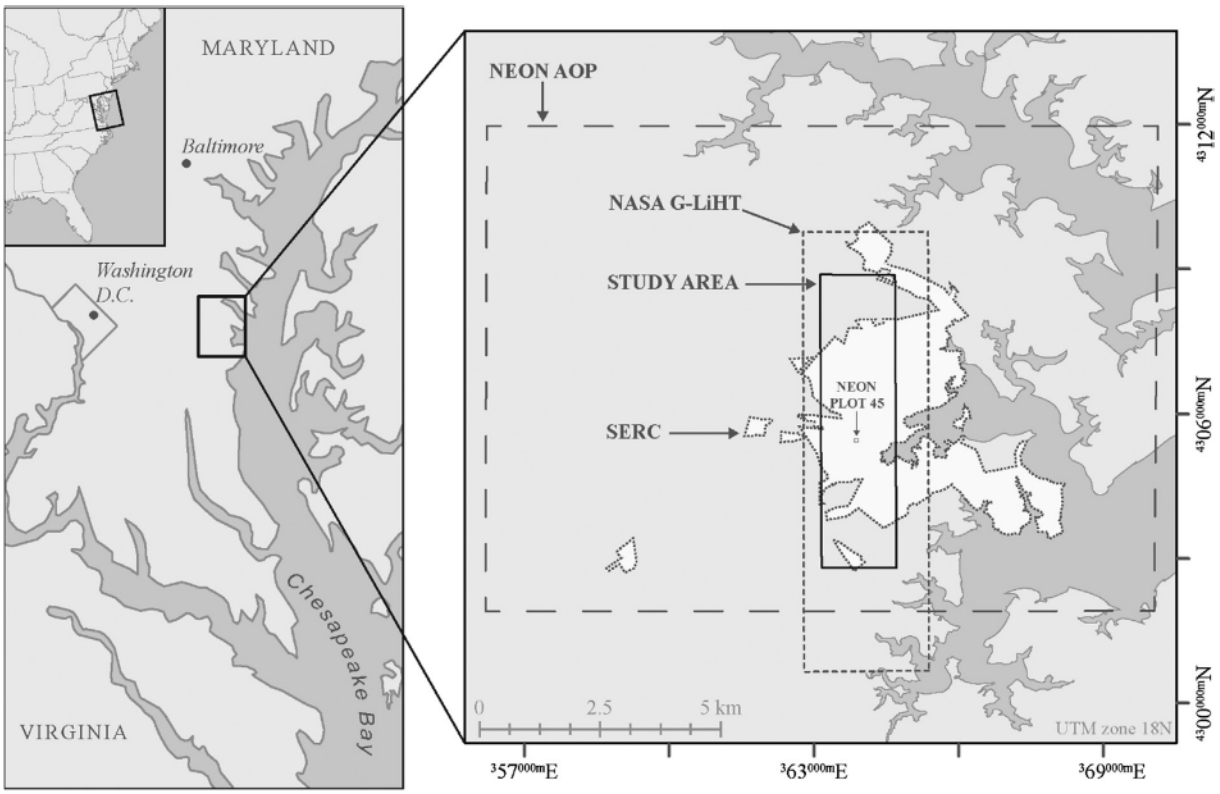

Fig. 1. The study area (solid line) is an overlapping subset of the NEON AOP (long dashed line) and NASA G-LiHT (short dashed line) flight boundaries. The noncontiguous boundary of SERC is shown in white with a dotted outline, while NEON plot 45 is shown by a small dashed box within the SERC boundary.

2.2. Hemispherical photography for LAI estimation

We collected hemispherical photographs between July 23 and August 7, 2017 to coincide with G-LiHT and NEON flights, using a Canon EOS Rebel T6 camera with an 8 mm circular fish-eye lens (180-degree angle of view). We placed the camera on a leveled tripod one meter above the ground to reduce the influence of ground vegetation and provide a vertical picture of the canopy. Each location was recorded using a Trimble GEO7x GPS. We took a single hemispherical photograph at 48 different locations along six transects and three plots within half a kilometer of the NEON flux tower (38.89° N, −76.56° W), with all photographs taken before sunrise or under uniformly cloudy conditions. Using the Digital Hemispherical Photography (DHP) software (Leblanc et al., 2005), we processed the hemispherical photographs for effective plant area index (PAIe), which includes leaf and woody material in the gap fraction calculation (Miller, 1967). Most studies use PAIe as a proxy for LAI due to the difficulty of correcting for non-foliage elements in these photographs (Richardson et al., 2009), and hereafter we refer to PAIe as LAI. Further, we set the zenith angle within the DHP software to match the scanning angle of each LiDAR sensor, to better relate the ground measured LAI to LiDAR derived LAI (Sabol et al., 2014; Richardson et al., 2009; Solberg et al., 2006; Korhonen et al., 2011).

2.3. LiDAR acquisition and processing

NASA G-LiHT and NEON AOP collected LiDAR data on July 31, 2017 and between July 20 and August 10, 2017, respectively. NASA G-LiHT data were collected using a Riegl VQ-480i LiDAR sensor, operating at a wavelength of 1550 nm, with a scan angle of ± 30 degrees, a pulse repetition frequency of 300 kHz, a beam divergence of 0.3 mRad, and an average point density of 15.86 pts/m^2. NEON AOP data were collected using an ALTM Gemini LiDAR sensor, operation at a wavelength of 1064 nm, with a scan angle of ± 18 degrees, a pulse repetition frequency (PRF) of 100 kHz, a beam divergence of 0.8 mRad, and an average point density of 3.15 pts/m^2. Differences in the specifications of LiDAR systems can have substantial impacts on subsequent LAD and LAI estimations. Below we describe these parameters and how they relate to measuring forest canopies.

The scan angle is the range of angles at which the sensor scans the landscape (Fig. 2A). By increasing the scan angle, the LiDAR pulses will cover a larger area and have a greater change of encountering a gap in the canopy, thus having a higher probability of penetrating a dense forest canopy. The pulse repetition frequency (PRF; Fig. 2C) is the number of pulses per second that a sensor produces, measured in cycles per second or kilohertz (kHz). A lower PRF results in fewer pulses produced per second, thus negatively affecting the density of the point cloud and the probability of penetrating a dense canopy. A related measure is beam divergence (Fig. 2B), which is an angular measure describing how the laser beam widens as the distance between the sensor and the ground grows, measured in milliradians (mRad). A large mRad value will cause the laser's energy to be spread across a wider area, likely reducing its ability to penetrate a dense forest canopy and producing a lower signal-to-noise ratio (Gatziolis and Andersen, 2008). Together, these parameters are pivotal to producing a high-quality LiDAR dataset with precise and accurate information about the internal structure of the forest canopy. Combined, these parameters determine point cloud density, forest canopy penetration, and the proportion of ground returns in the dataset, the latter of which is an essential measurement in the estimation of LAI and LAD.

We downloaded LiDAR point clouds as .las and .laz files through the NEON (National Ecological Observatory Network, 2017) and NASA (Cook et al., 2013) data portals. LiDAR pulses within the point cloud were classified as ground or not-ground by NEON and NASA prior to downloading. The code to reproduce these analyses is available as an R package on GitHub (canopyLazR; see Data Availability Statement). Using the R programming language (R Core Team, 2016), we loaded the LiDAR files into the workspace as individual datasets using the rlas

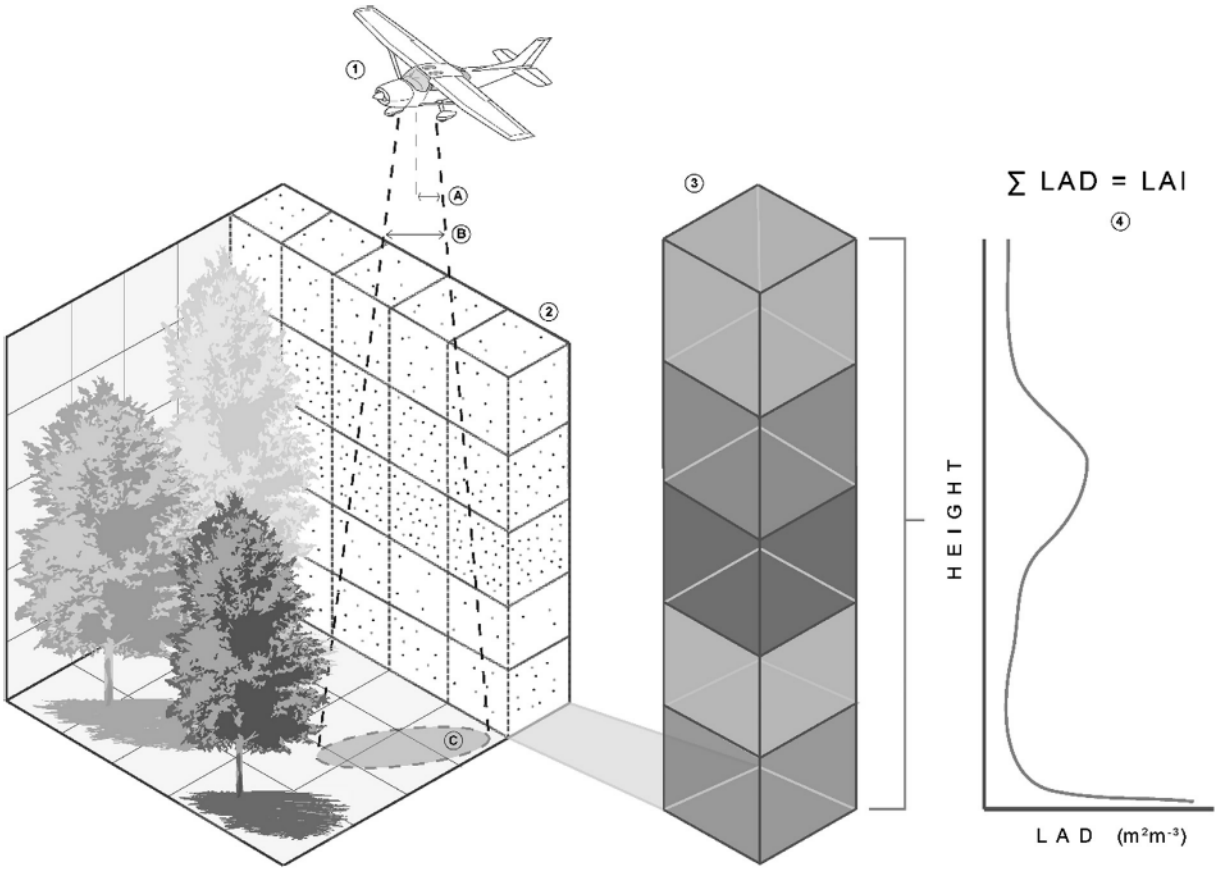

Fig. 2. LiDAR pulses from the airborne sensor penetrate the forest canopy and either bounce off leaf or woody material, or hit the ground, and return to the plane (1). These height measurements are then voxelized at the desired spatial resolution (2). The MacArthur and Horn method is then applied to voxelized columns of LiDAR returns (3) returning a LAD profile of the given area (4). The sum of LAD values in a column of voxels with a ground return is equal to the LAI of that vertical column. Further, the scan angle (A), beam divergence (B), and point density (C) sensor-survey parameters are highlighted.

library (Roussel, 2016). Due to the different spatial footprints of the NEON AOP and NASA G-LiHT flights, we took a subset of the overlapping data, thus returning two datasets (NEON AOP and NASA G-LiHT) with matching spatial extents, each with an area of 7.2 km^2 (Fig. 1). Next, we transformed the point clouds into voxelized arrays using the R libraries plyr (Wickham, 2011) and fields (Nychka et al., 2015). The first slice of the voxelized array contains the lowest ground height for each column of voxels. While using the lowest ground height might introduce some amount of uncertainty (Khosravipour et al., 2015), we choose the lowest ground height rather than the mean ground height so that we would not eliminate any understory vegetation that occurred below the mean ground elevation. The next slice contains the height of the canopy and each subsequent slice contains the number of pulses that occur in the given voxel. We set the voxel height to one meter, but used multiple horizontal resolutions for this study: 1 × 1 m, 2 × 2 m, 5 × 5 m, 10 × 10 m, 20 × 20 m (NEON vegetation plot resolution; National Ecological Observatory Network, 2017), and 30 × 30 m (Landsat pixel resolution). If there is not a ground return present in the vertical column, we assigned it a NA value, and this column was not used in subsequent analyses. We removed these voxels because we wanted to account for the total canopy LAD and not just the upper canopy. In addition, the data were voxelized at each of these spatial resolutions independently, not by aggregating finer resolutions together. For instance, a 10 × 10 m voxel contains all LiDAR returns that occur within the given spatial extent, whereas aggregating finer spatial resolutions together would result in the removal of many voxels that have upper canopy returns but no ground returns, which would result in a NA value for the entire vertical column. To better compare the voxelized data independent of changes in topography across the study site, we created a voxelized canopy height model from the LiDAR array so that each column of voxels was scaled to the distance from the ground, thus the ground has a height of zero. This eliminates the effects of topography on the dataset making comparisons between voxel columns easier (Lovell et al., 2003).

2.4. Leaf area density from airborne LiDAR

We estimated LAD from voxelized LiDAR data using an approach based on the method established by MacArthur and Horn (1969) and similar to other published methods (Stark et al., 2012; Zhao and Popescu, 2009; Solberg et al., 2006; Sumida et al., 2009; Bouvier et al., 2015) (Fig. 2). With this methodology, we calculated LAD by counting the number of LiDAR pulses that enter and exit each voxel in a given vertical column. Within each voxel, LAD is estimated as:

$$LAD_{i-1,i} = ln\left(\frac{S_e}{S_t}\right)\frac{1}{k\Delta z}$$

where for each vertical column of voxels, i is a voxel in a sequentially ordered vertical column of the canopy, S_e is the number of pulses entering the given voxel, S_t is the number of pulses exiting the same voxel, k is an extinction coefficient, and z represents the height of a voxel. The term k represents a Beer-Lambert Law extinction coefficient, which describes the attenuation of light by a medium or an object. When applied to forest canopies this derived value includes a correction for the non-random distribution and orientation of the foliage and the thickness of the leaf material and the forest canopy. Thus, as the canopy becomes denser and more leaves are encountered, the penetration of LiDAR pulses will diminish causing sample sizes for estimating LAD to

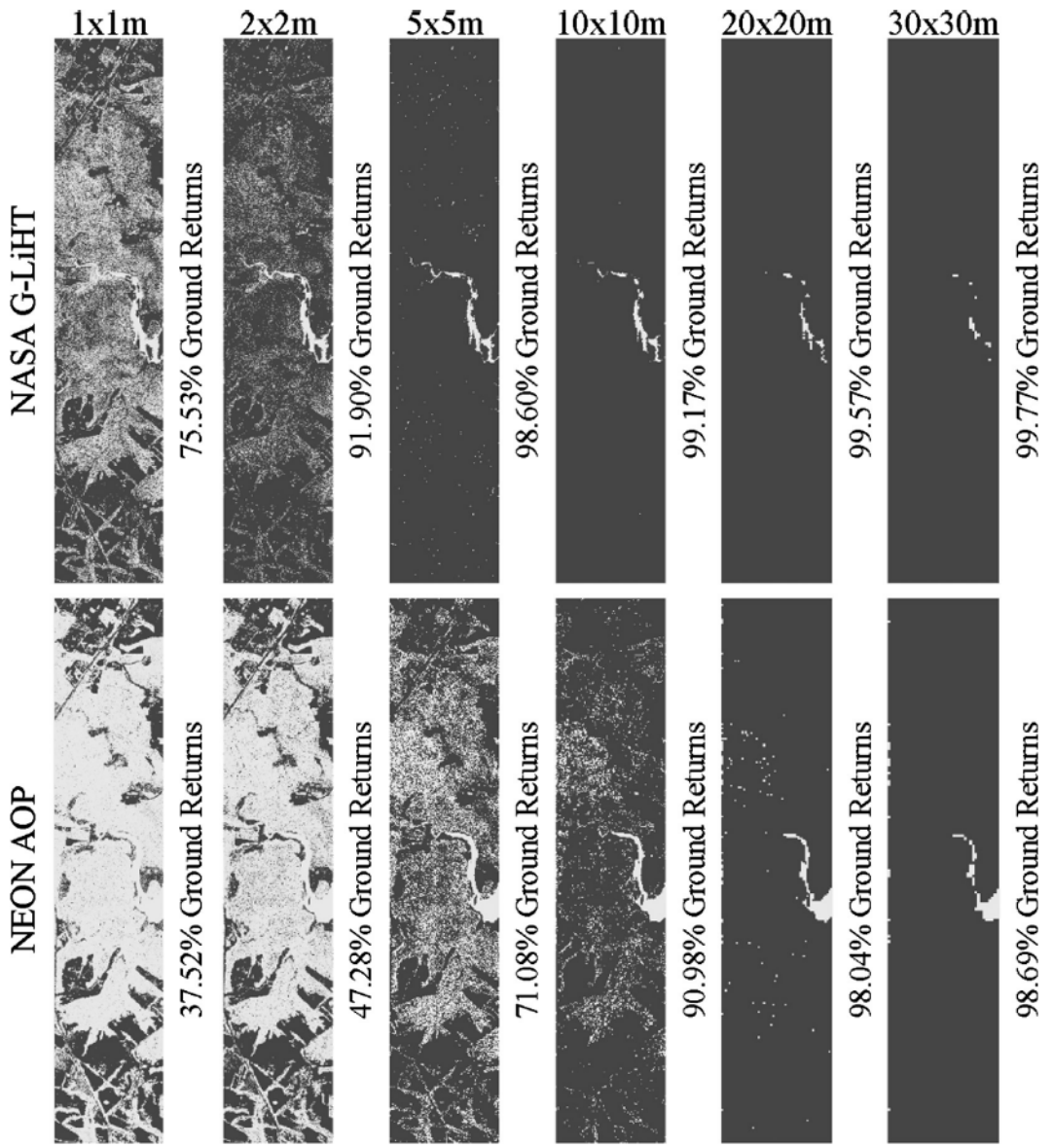

Fig. 3. Six different spatial resolutions were used for this study, which are shown here. The percentage of ground returns for each spatial resolution are shown, which increase with the coarsening of spatial resolution. Black pixels are locations of ground returns and light gray pixels do not have ground returns.

decrease and error to increase.

An extinction coefficient can be used to better relate field measured LAI with LiDAR estimated LAD or LAI. To estimate the extinction coefficient, we first estimated LAD from the LiDAR data with the extinction coefficient set to one. We removed vertical columns of voxels without at least one ground return from further analysis since this indicates that some of the canopy column was not sampled by the LiDAR sensor, thus preventing estimation of LAD in unsampled voxels and LAI which relies on the sum of all column voxels. We then extracted the LiDAR estimated LAI values at the same coordinates the hemispherical photographs were taken, using the field recorded GPS locations. Next, we plotted each extracted LiDAR estimated LAI value against the same LAI estimate from a hemispherical photograph. The slope of the linear model fit without an intercept, which is used because the Beer-Lambert law assumes that there is a true zero intercept, estimates the extinction coefficient (Klingberg et al., 2017). We then estimated LAD from the LiDAR array again, this time including the extinction coefficient in the above equation, resulting in a LAD estimate for each voxel in a given vertical column that is adjusted to more closely resemble the hemispherical photography approach. We repeated this process for both sensors at each of the six spatial resolutions, resulting in 12 voxelized arrays containing LAD estimates.

2.5. LAD profile extraction

To extract LAD vertical profiles for individual point locations, we converted the adjusted LAD arrays to raster stacks with each raster layer representing a 1 m interval of the forest canopy using the raster package (Hijmans, 2016) in R. We then generated 50 random 20 × 20 m plots across the study area to compare LAD estimates from each of the airborne systems. At each plot, the mean LAD estimate of all raster cells, at all heights within the canopy, that were either completely or partially within the plot was extracted. We repeated this for each of the 12 raster stacks previously generated (each sensor and six spatial resolutions). To better visualize this information, we extracted this same data from a permanent NEON forest plot (NEON plot 45; see Fig. 1), using coordinates from the NEON data portal.

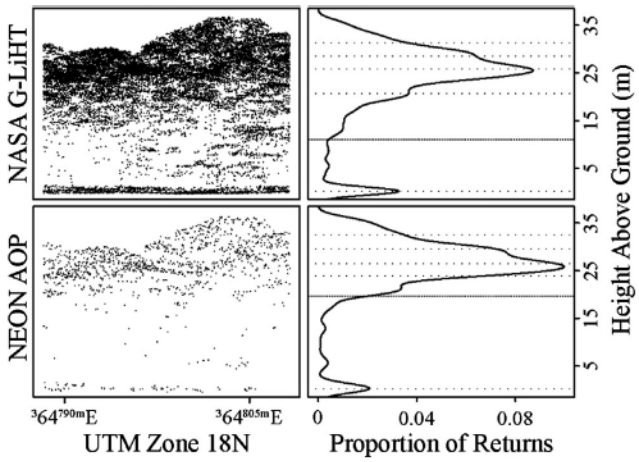

Fig. 4. We used a permanent 20 × 20 m NEON vegetation plot (NEON plot 45) to extract LiDAR point return information. The left plots show all LiDAR pulses within the plot, with NASA G-LiHT having 20,475 returns and the NEON AOP having 1299 returns within the same plot area. The right plots show the proportion of returns at each meter above the ground. The dotted lines show the ground (0 m), 10th percentile, 25th percentile, 50th percentile, 75th percentile, and 90th percentile. The 10th percentile is shown as a slightly darker dotted line to highlight the differences between sensors deep in the canopy.

Table 1
Beer-Lambert coefficients for each LiDAR sensor at each spatial resolution based on relationships with hemispherical photographs.

Beer-Lambert Coefficients						
	1 × 1	2 × 2	5 × 5	10 × 10	20 × 20	30 × 30
NASA G-LiHT	1.01	0.87	0.83	0.67	0.58	0.48
NEON AOP	1.34	1.12	0.85	0.68	0.63	0.56

2.6. Comparing LAD estimates

To compare the LAD estimates from NEON AOP and NASA G-LiHT, we used linear regression to model the relationship between the estimates from each sensor and each spatial resolution. We split the data into two categories, ground to the top of the canopy (TOC) (all data) and 10 m above the ground to TOC (removing understory data), due to inflated LAD values that may occur in the understory of the canopy at coarser spatial resolutions (Stark et al., 2012). We speculate that this happens due to topographic effects within a given cell, where the range of ground elevations is greater than the voxel height. Point returns from the understory vegetation at these higher elevations will be counted in a voxel higher in the canopy than where they actually occur, due to a cell containing only a single ground elevation. Moreover, the vertical distribution of leaf area can change with the age of a forest stand, causing higher LAD values in the understory of younger and older stands, with LAD values peaking in the upper canopy in middle-aged stands (Brown and Parker, 1994). While 10 m might not be the best height to address LAD estimate uncertainty for a single spatial resolution, we chose this value to easily compare results across multiple spatial resolutions; studies conducted with a single spatial resolution should choose a height cutoff based on the data present. Next, we calculated R^2, 95% confidence intervals, lines of best fit, slopes, and Spearman's ρ, along with standard deviations for LAD estimations for each of the 6 spatial resolutions using the R programming language.

2.7. Comparing LAI and total leaf area estimates

To compare LAD estimates across the landscape, we calculated the mean LAI and total leaf area across the study area (TLA, km^2) by taking the sum of all LAI estimates across the study area. We did this for only the 10 × 10 m resolution, because it was the finest resolution that produced the most stable results between sensors. Due to the NEON AOP data having a large number of pixels with no ground returns, and thus a larger number of NA values, our estimates are slightly biased when compared to NASA G-LiHT. We have left these NA values in the analysis to better represent the results one could achieve if only a single data set was available. To better understand the differences between sensor estimates, we calculated LAI and TLA for three height subsets: ground to TOC, 10–20 m above the ground, and 20 m above the ground to TOC. We calculated the mean difference in LAI across the study area and between each sensor by calculating the mean of absolute values at each pixel of NASA G-LiHT LAI minus NEON AOP LAI. We also calculated the difference in TLA between each sensor by taking the difference in TLA estimates from NASA G-LiHT and NEON AOP. We calculated the percent difference by subtracting the NEON AOP values from the G-LiHT values and dividing by G-LiHT values. While mean LAI and TLA yield similar results, particularly if LAI values are normally distributed, here we present both, as mean LAI represents the average expected value at the local scale, while TLA represents the aggregated leaf area across the landscape. While TLA across a landscape may seem overly coarse for studies of fine scale variation in forest structure, TLA measurements will connect to scales relevant to global land surface models and eddy covariance towers.

3. Results

3.1. LiDAR penetration of forest canopies

LiDAR ground return counts increase with the coarsening of spatial resolution for both the NASA G-LiHT and NEON AOP platforms (Fig. 3). However, there were notable differences between the two systems at finer spatial resolutions. At a 1 × 1 m resolution within the study area, NASA G-LiHT had ground returns in 75.53% of the raster cells, while NEON AOP had 37.52%. While differences persist, both sensors were within 10% of each other at a 10 × 10 m resolution where NASA G-LiHT had 99.17% ground returns and NEON AOP had 90.98% ground returns.

These two airborne systems also exhibit differences in the depth of canopy penetration (Fig. 4). Within NEON plot 45, a 20 × 20 m NEON vegetation plot, NASA G-LiHT had 20,475 LiDAR returns while NEON AOP had 1299, or 94% less returns than NASA G-LiHT. When we binned these returns by height, the 25th, 50th, 75th, and 90th percentiles occurred at similar heights above the ground. However, the 10th percentile of returns for NASA G-LiHT occurred much deeper in the canopy at 11.5 m above the ground, while the 10th percentile of returns for NEON AOP occurred at 20.3 m above the ground. These findings highlight the differences in canopy penetration between the two sensors, as the distribution of LiDAR returns is skewed more deeply into the canopy in the G-LiHT data.

3.2. Beer-Lambert coefficients

Using the field-measured LAI together with the LiDAR LAI estimates, we calculated a broad range of Beer-Lambert coefficients at different spatial resolutions (Table 1). We found that Beer-Lambert coefficients decrease with the coarsening of spatial resolutions regardless of airborne system. These coefficients approach 0.5, which is commonly used in closed-canopy forest ecosystems (Stark et al., 2012; Vose et al., 1995; Burton et al., 1991), at these coarser spatial resolutions.

3.3. LAD profile estimates

We observed a general increase in the agreement between NASA G-LiHT and the NEON AOP LAD values with coarsening spatial resolution

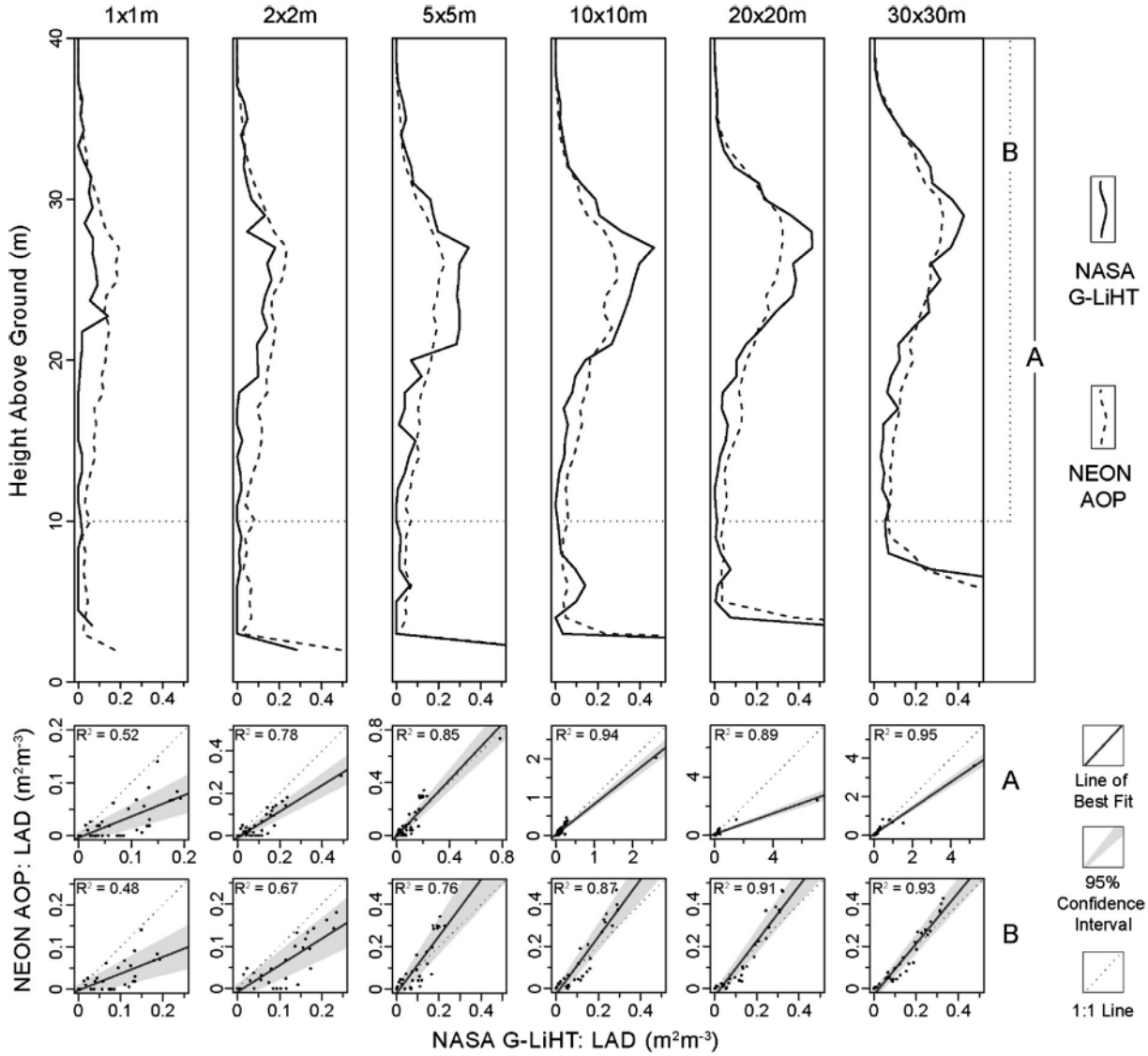

Fig. 5. All spatial resolutions considered are shown for NEON Plot 45 with NASA G-LiHT and NEON AOP LAD profiles in the first row of plots. LAD values were cut off at 0.5 for visualization, so that differences in the upper canopy can be seen. Plots in row A show the relationship between NASA G-LiHT and NEON AOP LAD data at each spatial resolution from the ground to TOC. Plots in row B, show the same relationship, but only including data from 10 m above ground to TOC. All R^2 values are significant at $p < 0.001$.

Table 2
LAD profiles (for all voxels) for 50 random 20 × 20 m plots from each spatial resolution and for each sensor (NASA and NEON) were extracted. For every plot at each spatial resolution and for each sensor, R^2, RMSE, and slope were calculated from a linear regression. Spearman's ρ was also calculated. SD = standard deviation.

LAD Estimates: Ground to Top of Canopy												
	1 × 1		2 × 2		5 × 5		10 × 10		20 × 20		30 × 30	
	Mean	SD	Mean	SD	Mean	SD	Mean	SD	Mean	SD	Mean	SD
R^2	0.66	0.27	0.76	0.19	0.85	0.17	0.89	0.15	0.95	0.07	0.93	0.10
RMSE	0.01	0.01	0.02	0.01	0.03	0.02	0.05	0.04	0.05	0.05	0.08	0.07
Slope	0.36	0.23	0.53	0.22	0.91	0.38	1.04	0.52	1.22	1.26	0.91	0.46
Spearman's ρ	0.83	0.13	0.90	0.08	0.95	0.04	0.97	0.05	0.97	0.05	0.98	0.03

in both sets of data (ground to TOC and 10 m above the ground to TOC) (Fig. 5). When the entire dataset is considered (row A, Fig. 5), R^2 values increase and the 95% confidence interval becomes narrower as the spatial resolution becomes coarser while the line of best fit changes drastically based on the position of the spuriously large values in the lower canopy, as discussed in Section 2.6. However, while row B in Fig. 5 (10 m above ground to TOC) shows a similar loosely correlated relationship at finer spatial resolutions and R^2 values increasing as the spatial resolution becomes coarser, the line of best fit approaches the 1:1 line as the spatial resolution coarsens, signifying a stronger relationship between these two datasets. The tightening of this relationship begins to occur at a 10-meter spatial resolution ($R^2 = 0.87$), which is also the spatial resolution where over 90% of cells have a ground return value in both datasets.

Table 3
LAD profiles (for voxels 10 m above the ground to TOC) for 50 random 20 × 20 m plots from each spatial resolution and for each sensor (NASA and NEON) were extracted. For every plot at each spatial resolution and for each sensor, R^2, RMSE, and slope were calculated from a linear regression. Spearman's ρ was also calculated. SD = standard deviation.

LAD Estimates: 10 Meters Above Ground to Top of Canopy												
	1 × 1		2 × 2		5 × 5		10 × 10		20 × 20		30 × 30	
	Mean	SD	Mean	SD	Mean	SD	Mean	SD	Mean	SD	Mean	SD
R^2	0.55	0.22	0.67	0.17	0.83	0.13	0.90	0.05	0.93	0.05	0.91	0.08
RMSE	0.01	0.01	0.02	0.02	0.02	0.02	0.02	0.02	0.02	0.01	0.02	0.01
Slope	0.35	0.19	0.46	0.22	1.01	0.29	1.08	0.31	1.05	0.22	0.92	0.21
Spearman's ρ	0.76	0.18	0.80	0.18	0.93	0.05	0.94	0.11	0.98	0.02	0.96	0.06

To consider the broader landscape variation and patterns, we generated 50 random 20 × 20 plots and extracted the same data as in the case of NEON Plot 45. At these 50 randomly located plots, we observed the same general relationships described above when all the data from the ground to TOC were employed (Table 2) and when only the data from 10 m above the ground to the TOC were employed (Table 3). These findings show that NEON Plot 45 is not an anomaly and instead is representative of the relationships between these two LiDAR datasets across the landscape.

3.4. Total leaf area estimates

Across the entire study area, results reflect our findings at the plot level (Fig. 6). From 20 m to TOC, NEON AOP has slightly higher LAI and TLA estimates than NASA G-LiHT due to the point cloud being skewed towards the top of canopy. Even with these differences, there was less than a 5% difference in TLA between the two sensors at this height interval. Between 10 and 20 m above the ground, there was a 10% difference between in TLA between the sensors, with NASA G-LiHT having slightly higher estimates due to the point cloud being skewed lower in the canopy than NEON AOP. When 10 m above the ground to TOC is considered, there is a 2% difference between TLA estimates between the two sensors. However, when the ground to top of canopy is considered there is a much larger difference between TLA estimates at 17%.

4. Discussion

4.1. Measuring leaf area density from above

While there are differences between these two airborne systems, our analysis can serve as a case study on how to estimate LAD at the appropriate spatial resolution for a given airborne LiDAR data set. Since these total canopy calculations are limited by the need to have a ground return in a given raster cell, this is often the most significant limiting factor in the estimation of LAD. The lack of ground returns can severely limit the spatial coverage of LAD estimates across the landscape, which can result in missing data within the study area, thus finding a balance between spatial resolution and spatial coverage is often the first step in these calculations. While it would be ideal to compare these datasets for other research sites, this is often not possible because only one of the datasets is available for a given area, thus the need to have comparable LAD estimates between sensors. By excluding voxels that lack ground returns we ensure that the entire canopy is accounted for in our LAD estimates, while providing forest structural estimates at an ecologically relevant scale (10 × 10 m is similar to a canopy dominant tree crown) to help answer landscape- and macro-scale questions.

We have shown that even low pulse density NEON AOP LiDAR data can be used to successfully estimate LAD, but these measurements come at the expense of spatial resolution. LAD estimates from between sensors began to stabilize at around a 10-meter resolution; however, there is still the need to remove a portion of the understory for close agreement, likely due to errors related to topographic changes inflating LAD estimates near the ground. Such understory inflation is particularly evident with NASA G-LiHT due to its high pulse density and canopy penetration. On the other hand, because of this high pulse density and canopy penetration LAD estimates from NASA G-LiHT can be calculated at finer spatial resolutions, allowing for the consideration of the full LAD profile. However, there is a tradeoff between high data density (NASA G-LiHT) and spatial extent and temporal coverage (NEON AOP). With NEON AOP flying the same sites on a semiannual basis, the ability to have yearly, landscape scale analyses might outweigh the need for finer resolutions of LAD estimates. While NASA G-LiHT has a higher pulse density and greater canopy penetration, which allows for finer resolution analysis, traditionally the flights have covered smaller areas, are not conducted on a yearly basis, and are project driven. That said, the G-LiHT archive is extensive with data in over 30 US states and territories and several countries at the time of this study (https://gliht.gsfc.nasa.gov/), highlighting the potential to generate broad spatial estimates across a range of vegetation types at fine spatial scales.

We show that the low-density point cloud from the NEON AOP can be used to estimate LAD within the forest canopy, with minimal differences (around 2%), as long as the inflated understory estimates are removed. While removing the understory of the canopy from the dataset is not ideal, the temporal and spatial coverage of the NEON AOP provide a unique opportunity to monitor forest ecosystems in ways that were not previously possible. Additionally, our LAD estimates per voxel from 10 m above the ground to the top of canopy are within the ranges found by other research conducted at SERC (LAI of 4–7; LAD of 0.1–0.5) using field-based techniques (Parker and Tibbs, 2003; Brown and Parker, 1994). This offers additional evidence that we can obtain accurate LAD estimates from airborne LiDAR systems with differing parameters and from point clouds with varying degrees of density and canopy penetration. While we show that these measurements are accurate in the dense forests of SERC, more research is needed in different biomes to further test the abilities of airborne LiDAR to estimate LAD across landscapes.

4.2. LiDAR system considerations

All LiDAR collections are not the same. LiDAR sensor specifications (beam divergence, scan angle, etc.) have large impacts on the density and quality of the data and are tuned to the specific data collection goal. These specifications are important to consider before processing the data and can help the researcher determine how to best use the data. Specifications such as scan angle determine how LAI estimates from hemispherical photographs need to be constrained during processing (see Section 2.2), while beam divergence and pulse repetition frequency can help determine the quality of the point cloud and canopy penetration. Likewise, differences in the wavelength the LiDAR sensor operates at can affect how pulses are reflected within the canopy. For instance, leaves typically have a higher reflectance at 1064 nm (NEON

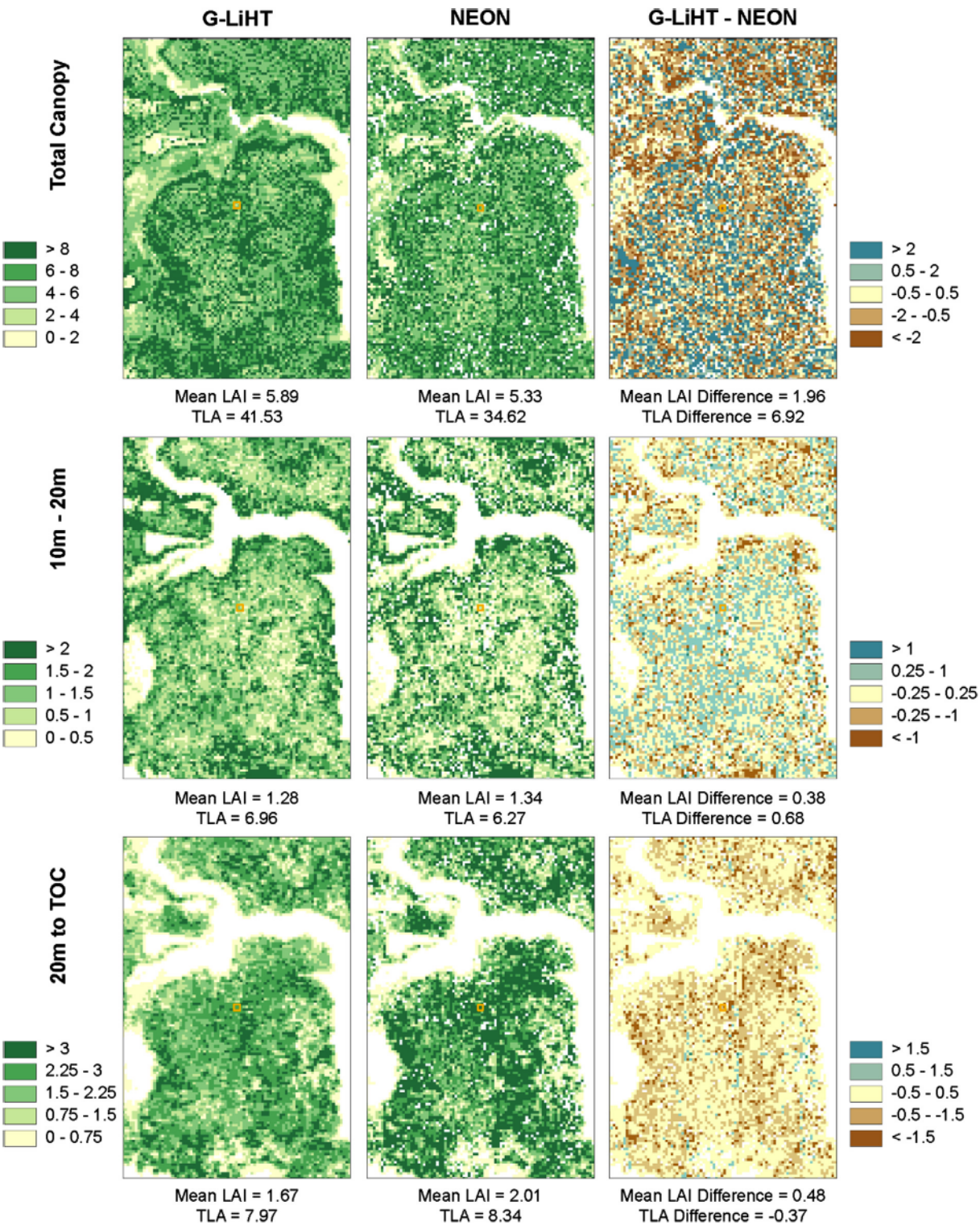

Fig. 6. Total leaf area (TLA; km^2) was estimated at three different canopy height intervals (ground to TOC, 10–20 m, 20 m to TOC, at the 10 × 10 m resolution across the entire study area. A subset of the study area is shown here for visualization purposes, but LAI and TLA values are calculated from the entire study area. Differences between the G-LiHT estimates and NEON estimates were also calculated. Mean LAI differences were calculated as the mean of the absolute values of the differences. NEON Plot 45 is shown as an orange square for reference. TLA is the total km^2 of leaf for the study area (7.2 km^2, solid line in Fig. 1).

AOP) than at 1550 nm (NASA G-LiHT), while bark has a higher reflectance at 1550 nm; this could lead to bark and branches having a slightly higher impact on returned pulses for NASA G-LiHT and leaves having a slightly higher impact for the NEON AOP. While the extent of the impact due to these differences would be difficult to quantify without ray tracing and a well-defined architecture, this would most likely lead to slightly different point clouds if all other variables were held constant. Examining the underlying metadata and understanding what the goals of the data collection mission are can help determine how the resulting LiDAR data can be used for a specific research project. For example, we have shown here that NEON AOP LiDAR data are adequate for measuring LAD in the forest canopy at a 10-meter

resolution, but not for detecting variations in the understory if the understory is dense.

4.3. Ecological implications

While it would be ideal to use a spatial resolution that mimics the fine scale variation found within a forest canopy (e.g. 1 × 1 m), this may not always be possible due to data availability. Since the LiDAR data available for ecological studies differs from site to site, it is challenging to compare studies and combine analyses over such heterogeneous collections. By developing standardized approaches for LAD and LAI estimation that are accurate and consistent regardless of the sensor used, analyses can more easily compare multiple studies while encompassing varied data sources, resulting in an opportunity for robust quantitative comparison and hypothesis testing. We have shown that LAD and LAI estimates at 10 × 10 m, that are fine-tuned with hemispherical photographs, are in line with field-based measurements across two very different airborne LiDAR systems. Thus, we propose a resolution of 10 × 10 m to estimate LAD and LAI, with inflated understory LAD estimates removed, as a viable standard resolution for landscape to macro-scale studies that use LiDAR data collected with lower pulse densities (e.g. less than 20 pulses per m^2). While a 10 × 10 m resolution will not be fine enough to investigate leaf level processes or the structural components of individual trees, airborne LiDAR with moderate to low pulse densities is still well situated for the investigation of landscape to macro-scale trends. When higher pulse densities are available from airborne, ground, and drone based LiDAR systems, there is the potential to model biophysical processes occurring at the leaf level (Wu et al., 2018), to investigate the role of fine-scale heterogeneity on canopy function (Atkins et al., 2018), and to consider the structural components of individual trees (Hosoi and Omasa, 2006). As these types of high-density LiDAR data become more readily available, additional detailed analyses will be needed to quantify structural and functional processes at these finer scales.

4.4. Looking forward

With LiDAR data becoming more readily available, it is important to consider the end user and their needs. Airborne and spaceborne platforms like NASA G-LiHT, NEON AOP, and GEDI are collecting and will continue to collect a large catalog of LiDAR data across a variety of ecoregions, allowing researchers the opportunity to ask and answer new questions about forest structure at large spatial scales. To support these new lines of research, we present a reproducible workflow and encourage other researchers to do the same, so that the scientific community as a whole can use these data in a consistent and standardized manner. While there are many other approaches to estimating LAD from airborne LiDAR (e.g. McNeil et al., 2016; Detto et al., 2015), we have shown that our methodology produces accurate estimates that are based on well-established field-based methodologies. With this large influx of data, we have a unique opportunity to not only use LiDAR data in new ways, but also to incorporate the resulting products into research projects that may have never considered using LiDAR data previously.

5. Conclusion

LiDAR has become a common data type in the remote sensing community and with this large influx of data, there are many unique opportunities to incorporate it into different ecological studies. Here we have presented a reproducible methodology to produce LAD and LAI estimates from airborne LiDAR with R code available for other researchers to use. We also highlight the importance of airborne LiDAR survey parameters that dictate pulse return density and ultimately determine the coverage of LAD and LAI estimates within survey areas, while providing ideas on how this data can be used in ecological and forest studies. Furthermore, we show that a spatial resolution of 10 × 10 m can successfully estimate LAD with either of these two moderate to low pulse density airborne sensors. While LiDAR data has been used to inform management and conservation decisions related to the estimation of aboveground biomass and productivity (Hughes et al., 2018; Socha et al., 2017), the response of forests to large-scale disturbances (Hoffman et al., 2018), the impacts of drought on forest health (Paz-Kagan et al., 2018), and the conservation of biodiversity (Garabedian et al., 2017; Mao et al., 2018), these methodologies can be difficult to reproduce. To help bridge this gap between ecologists and forest managers who could use LiDAR data in research and management plans and remote sensing scientists who use this data on a regular basis, we provide an open source, reproducible, and standardized workflow to calculate LAD and LAI from airborne LiDAR data.

Acknowledgments

Thanks to Logan Brissette for field assistance and to the Smithsonian Environmental Research Center, especially Geoffrey Parker, Patrick Megonigal, and Sean McMahon, for providing site access and space. This work was supported in part by the NSF Macrosystem Biology Program award #1702379. The National Ecological Observatory Network is a program sponsored by the National Science Foundation and operated under cooperative agreement by Battelle Memorial Institute. NASA's G-LiHT is a program sponsored by the NASA Goddard Space Flight Center's Internal Research and Development program and NASA's Terrestrial Ecology, Carbon Cycle and Carbon Monitoring System programs. This material is based in part upon work supported by the National Science Foundation through the NEON Program. Shawn P. Serbin was partially supported by the United States Department of Energy contract No. DE-SC0012704 to Brookhaven National Laboratory.

Data availability

LiDAR point clouds are available at: http://data.neonscience.org and https://glihtdata.gsfc.nasa.gov. R package to estimate LAD and LAI from airborne LiDAR data is provided through GitHub at: https://github.com/akamoske/canopyLazR. Hemispherical photographs and shapefile with locations can be found on figshare at: https://doi.org/10.6084/m9.figshare.6955142.v1.

References

Anderegg, W.R.L., Kane, J.M., Anderegg, L.D.L., 2013. Consequences of widespread tree mortality triggered by drought and temperature stress. Nat. Clim. Change 3, 30–36. https://doi.org/10.1038/nclimate1635.

Antonarakis, A.S., Munger, J.W., Moorcroft, P.R., 2014. Imaging spectroscopy- and lidar-derived estimates of canopy composition and structure to improve predictions of forest carbon fluxes and ecosystem dynamics. Geophys. Res. Lett. 41, 2535–2542. https://doi.org/10.1002/2013GL058373.

Atkins, J.W., Fahey, R.T., Hardiman, B.S., Gough, C.M., 2018. Forest canopy structural complexity and light absorption relationships at the subcontinental scale. J. Geophys. Res. Biogeosci. 123, 1387–1405. https://doi.org/10.1002/2017JG004256.

Baldocchi, D.D., Hincks, B.B., Meyers, T.P., 1988. Measuring biosphere-atmosphere exchanges of biologically related gases with micrometeorological methods. Ecology 69, 1331–1340. https://doi.org/10.2307/1941631.

Becknell, J.M., Desai, A.R., Dietze, M.C., Schultz, C.A., Starr, G., Duffy, P.A., Franklin, J.F., Pourmokhtarian, A., Jall, J., Stoy, P.C., Binford, M.W., Boring, L.R., Staudhammer, C.L., 2015. Assessing interactions among changing climate, management, and disturbance in forests: a macrosystems approach. Bioscience 65, 263–274.

Bonan, G.B., Oleson, K.W., Fisher, R.A., Lasslop, G., Reichstein, M., 2012. Reconciling leaf physiological traits and canopy flux data: use of the TRY and FLUXNET databases in the Community Land Model version 4. J. Geophys. Res.Biogeosci. 117, n/a-n/a. https://doi.org/10.1029/2011JG001913.

Bonan, G.B., Williams, M., Fisher, R.A., Oleson, K.W., 2014. Modeling stomatal conductance in the earth system: linking leaf water-use efficiency and water transport along the soil–plant–atmosphere continuum. Geosci. Model Dev. 7, 2193–2222. https://doi.org/10.5194/gmd-7-2193-2014.

Bouvier, M., Durrieu, S., Fournier, R.A., Renaud, J.P., 2015. Generalizing predictive models of forest inventory attributes using an area-based approach with airborne LiDAR data. Remote Sens. Environ. 156, 322–334. https://doi.org/10.1016/j.rse.

2014.10.004.
Brown, M.J., Parker, G.G., 1994. Canopy light transmittance in a chronosequence of mixed-species deciduous forests. Can. J. For. Res. 24, 1694–1703.
Burton, A.J., Pregitzer, K.S., Reed, D.D., 1991. Leaf area and foliar biomass relationships in northern hardwood forests located along an 800 km acid deposition gradient. Forest Sci. 37, 1041–1059.
Chen, J.M., Black, T.A., 1992. Defining leaf area index for non-flat leaves. Plant, Cell Environ. 15, 421–429. https://doi.org/10.1111/j.1365-3040.1992.tb00992.x.
Collins, B.M., Everett, R.G., Stephens, S.L., 2011. Impacts of fire exclusion and recent managed fire on forest structure in old growth Sierra Nevada mixed-conifer forests. Ecosphere 2, art51. https://doi.org/10.1890/ES11-00026.1.
Cook, B., Corp, L., Nelson, R., Middleton, E., Morton, D., McCorkel, J., Masek, J., Ranson, K., Ly, V., Montesano, P., 2013. NASA Goddard's LiDAR, Hyperspectral and Thermal (G-LiHT) Airborne Imager. Remote Sens. 5, 4045–4066. https://doi.org/10.3390/rs5084045.
Detto, M., Asner, G.P., Muller-Landau, H.C., Sonnentag, O., 2015. Spatial variability in tropical forest leaf area density from multireturn lidar and modeling: Multireturn LiDAR and tropical forest. J. Geophys. Res. Biogeosci. 120, 294–309. https://doi.org/10.1002/2014JG002774.
Ellsworth, D.S., Reich, P.B., 1993. Canopy structure and vertical patterns of photosynthesis and related leaf traits in a deciduous forest. Oecologia 96, 169–178. https://doi.org/10.1007/BF00317729.
Falkowski, M.J., Evans, J.S., Martinuzzi, S., Gessler, P.E., Hudak, A.T., 2009. Characterizing forest succession with lidar data: an evaluation for the Inland Northwest, USA. Remote Sens. Environ. 113, 946–956. https://doi.org/10.1016/j.rse.2009.01.003.
Fisher, R.A., Koven, C.D., Anderegg, W.R.L., Christoffersen, B.O., Dietze, M.C., Farrior, C.E., Holm, J.A., Hurtt, G.C., Knox, R.G., Lawrence, P.J., Lichstein, J.W., Longo, M., Matheny, A.M., Medvigy, D., Muller-Landau, H.C., Powell, T.L., Serbin, S.P., Sato, H., Shuman, J.K., Smith, B., Trugman, A.T., Viskari, T., Verbeeck, H., Weng, E., Xu, C., Xu, X., Zhang, T., Moorcroft, P.R., 2018. Vegetation demographics in Earth System Models: a review of progress and priorities. Glob. Change Biol. 24, 35–54. https://doi.org/10.1111/gcb.13910.
Garabedian, J.E., Moorman, C.E., Peterson, M.N., Kilgo, J.C., 2017. Use of LiDAR to define habitat thresholds for forest bird conservation. For. Ecol. Manage. 399, 24–36.
Gatziolis, D., Andersen, H.-E., 2008. A guide to LIDAR data acquisition and processing for the forests of the Pacific Northwest. (No. PNW-GTR-768). U.S. Department of Agriculture, Forest Service, Pacific Northwest Research Station, Portland, OR. https://doi.org/10.2737/PNW-GTR-768.
Goodale, C.L., Apps, M.J., Birdsey, R.A., Field, C.B., Heath, L.S., Houghton, R.A., Jenkins, J.C., Kohlmaier, G.H., Kurz, W., Liu, S., Nabuurs, G.-J., Nilsson, S., Shvidenko, A.Z., 2002. Forest carbon sinks in the Northern. Hemisphere 9.
Gough, C.M., Hardiman, B.S., Nave, L.E., Bohrer, G., Maurer, K.D., Vogel, C.S., Nadelhoffer, K.J., Curtis, P.S., 2013. Sustained carbon uptake and storage following moderate disturbance in a Great Lakes forest. Ecol. Appl. 23, 1202–1215. https://doi.org/10.1890/12-1554.1.
Hanson, J.J., Lorimer, C.G., 2007. Forest structure and light regimes following moderate wind storms: implications for multi-cohort managment. Ecol. Appl. 17, 1325–1340. https://doi.org/10.1890/06-1067.1.
Hardiman, B.S., Bohrer, G., Gough, C.M., Vogel, C.S., Curtis, P.S., 2011. The role of canopy structural complexity in wood net primary production of a maturing northern deciduous forest. Ecology 92, 1818–1827. https://doi.org/10.1890/10-2192.1.
Hardiman, B.S., Gough, C.M., Halperin, A., Hofmeister, K.L., Nave, L.E., Bohrer, G., Curtis, P.S., 2013. Maintaining high rates of carbon storage in old forests: a mechanism linking canopy structure to forest function. For. Ecol. Manage. 298, 111–119. https://doi.org/10.1016/j.foreco.2013.02.031.
Hijmans, R.J., 2016. Raster: Geographic Data Analysis and Modeling. R package version 2.5-8. http://CRAN.R-project.org/package=raster.
Hinckley, E.-L.S., Bonan, G.B., Bowen, G.J., Colman, B.P., Duffy, P.A., Goodale, C.L., Houlton, B.Z., Marín-Spiotta, E., Ogle, K., Ollinger, S.V., Paul, E.A., Vitousek, P.M., Weathers, K.C., Williams, D.G., 2016. The soil and plant biogeochemistry sampling design for The National Ecological Observatory Network. Ecosphere 7, e01234. https://doi.org/10.1002/ecs2.1234.
Hoffman, K.M., Trant, A.J., Nijland, W., Starzomski, B.M., 2018. Ecological legacies of fire detected using plot-level measurements and LiDAR in an old growth coastal temperate rainforest. For. Ecol. Manage. 424, 11–20.
Hosoi, F., Omasa, K., 2006. Voxel-based 3-D modeling of individual tress for estimating leaf area density using high resolution portable scanning lidar. IEEE Trans. Geosci. Remote Sens. 44, 3610–3618.
Hosoi, F., Omasa, K., 2007. Factors contributing to accuracy in the estimation of the woody canopy leaf area density profile using 3D portable lidar imaging. J. Exp. Bot. 58, 3463–3473. https://doi.org/10.1093/jxb/erm203.
Hughes, R.F., Asner, G.P., Baldwin, J.A., Mascaro, J., Bufil, L.K.K., Knapp, D.E., 2018. Estimating aboveground carbon density across forest landscapes of Hawaii: combining FIA plot-derived estimates and airborne LiDAR. For. Ecol. Manage. 424, 323–337.
Hummel, S., Agee, J.K., 2003. Western spruce budworm defoliation effects of forest structure and potential fire behavior. Northwest Sci. 15, 1–49.
Jarvis, P.G., McNaughton, K.G., 1986. Stomatal control of transpiration: scaling up from leaf to region. Adv. Ecol. Res. 15, 1–49.
Kampe, T.U., Johnson, B.R., Kuester, M., Keller, M., 2010. NEON: the first continental-scale ecological observatory with airborne remote sensing of vegetation canopy biochemistry and structure. J. Appl. Remote Sens. 4, 1–24. https://doi.org/10.1117/1.3361375.
Kitajima, K., 2004. Variation in crown light utilization characteristics among tropical canopy trees. Ann. Bot. 95, 535–547. https://doi.org/10.1093/aob/mci051.
Khosravipour, A., Skidmore, A.K., Wang, T., Isenburg, M., Khoshelham, K., 2015. Effect of slope on treetop detection using a LiDAR canopy height model. ISPRS J. Photogramm. Remote Sens. 104, 44–52.
Klingberg, J., Konarska, J., Lindberg, F., Johansson, L., Thorsson, S., 2017. Mapping leaf area of urban greenery using aerial LiDAR and ground-based measurements in Gothenburg, Sweden. Urban For. Urban Greening 26, 31–40. https://doi.org/10.1016/j.ufug.2017.05.011.
Korhonen, L., Korpela, I., Heiskanen, J., Maltamo, M., 2011. Airborne discrete-return LIDAR data in the estimation of vertical canopy cover, angular canopy closure and leaf area index. Remote Sens. Environ. 115, 1065–1080.
Le Quéré, C., Moriarty, R., Andrew, R.M., Peters, G.P., Ciais, P., Friedlingstein, P., Jones, S.D., Sitch, S., Tans, P., Arneth, A., Boden, T.A., Bopp, L., Bozec, Y., Canadell, J.G., Chini, L.P., Chevallier, F., Cosca, C.E., Harris, I., Hoppema, M., Houghton, R.A., House, J.I., Jain, A.K., Johannessen, T., Kato, E., Keeling, R.F., Kitidis, V., Klein Goldewijk, K., Koven, C., Landa, C.S., Landschützer, P., Lenton, A., Lima, I.D., Marland, G., Mathis, J.T., Metzl, N., Nojiri, Y., Olsen, A., Ono, T., Peng, S., Peters, W., Pfeil, B., Poulter, B., Raupach, M.R., Regnier, P., Rödenbeck, C., Saito, S., Salisbury, J.E., Schuster, U., Schwinger, J., Séférian, R., Segschneider, J., Steinhoff, T., Stocker, B.D., Sutton, A.J., Takahashi, T., Tilbrook, B., van der Werf, G.R., Viovy, N., Wang, Y.-P., Wanninkhof, R., Wiltshire, A., Zeng, N., 2015. Global carbon budget 2014. Earth Syst. Sci. Data 7, 47–85. https://doi.org/10.5194/essd-7-47-2015.
Leblanc, S.G., Chen, J.M., Fernandes, R., Deering, D.W., Conley, A., 2005. Methodology comparison for canopy structure parameters extraction from digital hemispherical photography in boreal forests. Agric. For. Meteorol. 129, 187–207. https://doi.org/10.1016/j.agrformet.2004.09.006.
Lefsky, M.A., Cohen, W.B., Parker, G.G., Harding, D.J., 2002. Lidar remote sensing for ecosystem studies. Bioscience 52, 19. https://doi.org/10.1641/0006-3568(2002)052[0019:LRSFES]2.0.CO;2.
Lovell, J.L., Jupp, D.L.B., Culvenor, D.S., Coops, N.C., 2003. Using airborne and ground-based ranging lidar to measure canopy structure in Australian forests. Can. J. Remote Sens. 29, 607–622. https://doi.org/10.5589/m03-026.
MacArthur, R.H., Horn, H.S., 1969. Foliage profile by vertical measurements. Ecology 50, 802–804. https://doi.org/10.2307/1933693.
Mairota, P., Cafarelli, B., Didham, R.K., Lovergine, F.P., Lucas, R.M., Nagendra, H., Rocchini, D., Tarantino, C., 2015. Challenges and opportunities in harnessing satellite remote-sensing for biodiversity monitoring. Ecol. Inf. 30, 207–214. https://doi.org/10.1016/j.ecoinf.2015.08.006.
Mao, L., Dennett, J., Bater, C.W., Tompalski, P., Coops, N.C., Farr, D., Kohler, M., White, B., Stadt, J.J., Nielson, S.E., 2018. Using airborne laser scanning to predict plant species richness and assess conservation threats in the oil sands region of Alberta's boreal forest. Forest Ecol. Manage. 409, 29–37.
McNeil, B.E., Pisek, J., Lepisk, H., Flamenco, E.A., 2016. Measuring leaf angle distribution in broadleaf canopies using UAVs. Agric. Forest Meteorol. 218, 204–208.
Meir, P., Kruijt, B., Broadmeadow, M., Barbosa, E., Kull, O., Carswell, F., Nobre, A., Jarvis, P.G., 2002. Acclimation of photosynthetic capacity to irradiance in tree canopies in relation to leaf nitrogen concentration and leaf mass per unit area. Plant, Cell Environ. 25, 343–357. https://doi.org/10.1046/j.0016-8025.2001.00811.x.
Meng, R., Dennison, P.E., Zhao, F., Shendryk, I., Rickert, A., Hanavan, R.P., Cook, B.D., Serbin, S.P., 2018. Mapping canopy defoliation by herbivorous insects at the individual tree level using bi-temporal airborne imaging spectroscopy and LiDAR measurements. Remote Sens. Environ. 215, 170–183. https://doi.org/10.1016/j.rse.2018.06.008.
Miller, J., 1967. A formula for average foliage density. Aust. J. Bot. 15, 141. https://doi.org/10.1071/BT9670141.
Morsdorf, F., Kötz, B., Meier, E., Itten, K.I., Allgöwer, B., 2006. Estimation of LAI and fractional cover from small footprint airborne laser scanning data based on gap fraction. Remote Sens. Environ. 104, 50–61. https://doi.org/10.1016/j.rse.2006.04.019.
National Ecological Observatory Network, 2017. Data Products NEON.DP1.10058.001, NEON.DP1.30003.001. Provisional data downloaded from https://data.neonscience.org on 6 Nov 2017. Battelle, Boulder, CO, USA.
Niinemets, Ü., 2007. Photosynthesis and resource distribution through plant canopies. Plant, Cell Environ. 30, 1052–1071. https://doi.org/10.1111/j.1365-3040.2007.01683.x.
Niinemets, Ü., Keenan, T.F., Hallik, L., 2015. A worldwide analysis of within-canopy variations in leaf structural, chemical and physiological traits across plant functional types. New Phytologist 205, 973–993. https://doi.org/10.1111/nph.13096.
Nychka, D., Furrer, R., Paige, J., Sain, S., 2015. Fields: Tools for spatial data. R package version 8.4-1. www.image.ucar.edu/fields.
Pan, Y., Birdsey, R.A., Fang, J., Houghton, R., Kauppi, P.E., Kurz, W.A., Phillips, O.L., Shvidenko, A., Lewis, S.L., Canadell, J.G., Ciais, P., Jackson, R.B., Pacala, S.W., McGuire, A.D., Piao, S., Rautiainen, A., Sitch, S., Hayes, D., 2011a. A large and persistent carbon sink in the world's forests. Science 333, 988–993. https://doi.org/10.1126/science.1201609.
Pan, Y., Chen, J.M., Birdsey, R., McCullough, K., He, L., Deng, F., 2011b. Age structure and disturbance legacy of North American forests. Biogeosciences 8, 715–732. https://doi.org/10.5194/bg-8-715-2011.
Parker, G.G., 1995. Structure and microclimate of forest canopies. In: Lowman, M., Nadkarni, N. (Eds.), Forest Canopies: A Review of Research on a Biological Frontier. Academic Press, San Diego, pp. 73–106.
Parker, G.G., Harmon, M.E., Lefsky, M.A., Chen, J., Pelt, R.V., Weis, S.B., Thomas, S.C., Winner, W.E., Shaw, D.C., Frankling, J.F., 2004. Three-dimensional structure of an old-growth pseudotsuga-tsuga canopy and its implications for radiation balance, microclimate, and gas exchange. Ecosystems 7. https://doi.org/10.1007/s10021-004-0136-5.
Parker, G.G., Tibbs, D.J., 2003. Structural phenology of the leaf community in the canopy

of a Liriodendron tulipifera L. Forest in Maryland, USA. Soc. Am. Foresters 11, 387–397.
Paz-Kagan, T., Vaughn, N.R., Martin, R.E., Brodrick, P.G., Stephenson, N.L., Das, A.J., Nydick, K.R., Asner, G.P., 2018. Landscape-scale variation in canopy water content of giant sequoias during drought. For. Ecol. Manage. 419–420, 291–304.
Pettorelli, N., Laurance, W.F., O'Brien, T.G., Wegmann, M., Nagendra, H., Turner, W., 2014. Satellite remote sensing for applied ecologists: opportunities and challenges. J. Appl. Ecol. 51, 839–848. https://doi.org/10.1111/1365-2664.12261.
Poorter, H., Niinemets, Ü., Poorter, L., Wright, I.J., Villar, R., 2009. Causes and consequences of variation in leaf mass per area (LMA): a meta-analysis. New Phytologist 182, 565–588. https://doi.org/10.1111/j.1469-8137.2009.02830.x.
Core Team, R., 2016. R: A Language and Environment for Statistical Computing. R Foundation for Statistical Computing, Vienna Austria. https://www.R-project.org.
Richardson, J.J., Moskal, L.M., Kim, S.-H., 2009. Modeling approaches to estimate effective leaf area index from aerial discrete-return LIDAR. Agric. For. Meteorol. 149, 1152–1160. https://doi.org/10.1016/j.agrformet.2009.02.007.
Roussel, J.R., 2016. Rlas: read and write 'las' and 'laz' binary file formats used for remote sensing data. R package version 1, 3. https://CRAN.R-project.org/package=rlas.
Roussel, J.R., Caspersen, J., Beland, M., Thomas, S., Achim, A., 2017. Removing bias from LiDAR-based estimates of canopy height: accounting for the effects of pulse density and footprint size. Remote Sens. Environ. 198, 1–16.
Sabol, J., Patočka, Z., Mikita, T., 2014. Usage of lidar data for leaf area index estimation. GeoSci. Eng. 60, 10–18. https://doi.org/10.2478/gse-2014-0013.
Serbin, S.P., Singh, A., McNeil, B.E., Kingdon, C.C., Townsend, P.A., 2014. Spectroscopic determination of leaf morphological and biochemical traits for northern temperate and boreal tree species. Ecol. Appl. 24, 1651–1669. https://doi.org/10.1890/13-2110.1.
Silva, C.A., Hudak, A.T., Vierling, L.A., Klauberg, C., Garcia, M., Ferraz, A., Keller, M., Eitel, J., Saatchi, S., 2017. Impacts of airborne lidar pulse density on estimating biomass stocks and changes in a selectively logged tropical forest. Remote Sens. 9, 1–19.
Smart, L.S., Swenson, J.J., Christensen, N.L., Sexton, J.O., 2012. Three-dimensional characterization of pine forest type and red-cockaded woodpecker habitat by small-footprint, discrete-return lidar. For. Ecol. Manage. 281, 100–110. https://doi.org/10.1016/j.foreco.2012.06.020.
Socha, J., Pierzchalski, M., Balazy, R., Ciesielski, M., 2017. Modelling top height growth and site index using repeated laser scanning data. For. Ecol. Manage. 406, 307–317.
Solberg, S., Næsset, E., Hanssen, K.H., Christiansen, E., 2006. Mapping defoliation during a severe insect attack on Scots pine using airborne laser scanning. Remote Sens. Environ. 102, 364–376. https://doi.org/10.1016/j.rse.2006.03.001.
Stark, S.C., Enquist, B.J., Saleska, S.R., Leitold, V., Schietti, J., Longo, M., Alves, L.F., Camargo, P.B., Oliveira, R.C., 2015. Linking canopy leaf area and light environments with tree size distributions to explain Amazon forest demography. Ecol. Lett. 18, 636–645. https://doi.org/10.1111/ele.12440.
Stark, S.C., Leitold, V., Wu, J.L., Hunter, M.O., de Castilho, C.V., Costa, F.R.C., McMahon, S.M., Parker, G.G., Shimabukuro, M.T., Lefsky, M.A., Keller, M., Alves, L.F., Schietti, J., Shimabukuro, Y.E., Brandão, D.O., Woodcock, T.K., Higuchi, N., de Camargo, P.B., de Oliveira, R.C., Saleska, S.R., 2012. Amazon forest carbon dynamics predicted by profiles of canopy leaf area and light environment. Ecol. Lett. 15, 1406–1414. https://doi.org/10.1111/j.1461-0248.2012.01864.x.
Stavros, E.N., Schimel, D., Pavlick, R., Serbin, S., Swann, A., Duncanson, L., Fisher, J.B., Fassnacht, F., Ustin, S., Dubayah, R., Schwigher, A., Wennberg, P., 2017. ISS observations offer insights into plant function. Nat. Ecol. Evol. 1, 1–4.
Sumida, A., Nakai, T., Yamada, M., Ono, K., Uemura, S., Hara, T., 2009. Ground-based estimation of leaf area index and vertical distribution of leaf area density in a Betula ermanii forest. Silva Fennica 43.
Taylor, P., Asner, G., Dahlin, K., Anderson, C., Knapp, D., Martin, R., Mascaro, J., Chazdon, R., Cole, R., Wanek, W., Hofhansl, F., Malavassi, E., Vilchez-Alvarado, B., Townsend, A., 2015. Landscape-scale controls on aboveground forest carbon stocks on the Osa Peninsula, Costa Rica. PLOS ONE 10, e0126748. https://doi.org/10.1371/journal.pone.0126748.
Turner, W., Rondinini, C., Pettorelli, N., Mora, B., Leidner, A.K., Szantoi, Z., Buchanan, G., Dech, S., Dwyer, J., Herold, M., Koh, L.P., Leimgruber, P., Taubenboeck, H., Wegman, M., Wikelski, M., Woodcock, C., 2015. Free and open-access to satellite data are key to biodiversity conservation. Biol. Conserv. 182, 173–176.
Vose, J.M., Sullivan, N.H., Clinton, B.D., Bolstad, P.V., 1995. Vertical leaf area distribution, light transmittance, and application of the Beer-Lambert Law in four mature hardwood stands in the southern appalachians. Can. J. For. Res. 25, 1036–1043.
Weiss, M., Baret, F., Smith, G.J., Jonckheere, I., Coppin, P., 2004. Review of methods for in situ leaf area index (LAI) determination. Agric. For. Meteorol. 121, 37–53. https://doi.org/10.1016/j.agrformet.2003.08.001.
Wickham, H., 2011. The split-apply-combine strategy for data analysis. J. Stat. Softw. 40, 1–29.
Wilson, J.W., 1960. Inclined point quadrats. New Phytol. 59, 1–7. https://doi.org/10.1111/j.1469-8137.1960.tb06195.x.
Wu, J., Kobayashi, H., Stark, S.C., Meng, R., Guan, K., Tran, N.N., Gao, S., Yang, W., Restrepo-Coupe, N., Miura, T., Oliviera, R.C., 2018. Biological processes dominate seasonality of remotely sensed canopy greenness in an Amazon evergreen forest. New Phytol. 217 (4), 1507–1520.
Zhao, K., Popescu, S., 2009. Lidar-based mapping of leaf area index and its use for validating GLOBCARBON satellite LAI product in a temperate forest of the southern USA. Remote Sens. Environ. 113, 1628–1645. https://doi.org/10.1016/j.rse.2009.03.006.
Zheng, G., Moskal, L.M., 2009. Retrieving leaf area index (LAI) using remote sensing: theories, methods and sensors. Sensors 9, 2719–2745. https://doi.org/10.3390/s90402719.